DNS study of decaying homogeneous isotropic turbulence with polymer additives

W.-H. CAI, F.-C. LI† AND H.-N. ZHANG

School of Energy Science and Engineering, Harbin Institute of Technology, Harbin 150001, China

In order to investigate the turbulent drag reduction phenomenon and understand its mechanism, direct numerical simulation (DNS) was carried out on decaying homogeneous isotropic turbulence (DHIT) with and without polymer additives. We explored the polymer effect on DHIT from the energetic viewpoint, i.e. the decay of the total turbulent kinetic energy and energy distribution at each scale in Fourier space and from the phenomenological viewpoint, i.e. the alterations of vortex structures, the enstrophy and the strain. It was obtained that in DHIT with polymer additives the decay of the turbulent kinetic energy is faster than that in the Newtonian fluid case and a modification of the turbulent kinetic energy transfer process for the Newtonian fluid flow is observed due to the release of the polymer elastic energy into flow structures at certain small scales. Besides, we deduced the transport equations of the enstrophy and the strain, respectively, for DHIT with polymer additives. Based on the analyses of these transport equations, it was found that polymer additives depress both the enstrophy and the strain in DHIT as compared to the Newtonian fluid case, indicating the inhibition effect on small-scale vortex structures and turbulence intensity by polymers.

Key words: drag reduction, isotropic turbulence, viscoelasticity

---

1. Introduction

The so-called Toms effect was discovered in 1949 (Toms 1949). It says that adding a minute amount of long-chain polymer or some kinds of surfactant additives into a turbulent liquid flow in a pipe or channel may cause a dramatic frictional drag reduction (DR). The DR rate can even be more than 80 %. The Toms effect has great potential in industrial applications, such as in saving pumping power in a water-circulating device such as a district heating/cooling system, long-distance liquid transportation pipeline systems, etc. To interpret this intriguing phenomenon of turbulent DR, many researchers have paid much attention to theoretical, experimental and numerical simulation studies on drag-reducing flows by additives.

During the last several decades, some theories about the mechanism of turbulent DR have been proposed (e.g. Lumley 1973; De Angelis, Casciola & Piva 2002*a*; Ptasinski *et al.* 2003). In these theories, the presence of a wall plays a major role. A great wealth of experimental studies have also been carried out on turbulent drag-reducing channels, pipe or boundary-layer flows with polymer or surfactant

---

† Email address for correspondence: lifch@hit.edu.cn

additives, particularly after the emergence of modern experimental techniques such as laser-Doppler velocimetry (e.g. Walker & Tiederman 1990; Den Toonder *et al.* 1997; Sreenivasan & White 2000; Ptasinski *et al.* 2001, 2003; Li, Kawaguchi & Hishida 2004) and particle image velocimetry (e.g. Warholic *et al.* 2001; Liberatore *et al.* 2004; Li *et al.* 2005, 2006; Cai *et al.* 2009). On the other hand, the investigation of turbulent DR mechanisms has flourished significantly with the development of computational fluid dynamics techniques, particularly direct numerical simulation (DNS) for wall-bounded turbulent drag-reducing flows (e.g. Den Toonder *et al.* 1997; Sureshkumar, Beris & Handler 1997; Beris & Dimitropoulos 1999; Min, Yoo & Choi 2001; Ptasinski *et al.* 2003; Yu & Kawaguchi 2004).

In spite of the extensive theoretical, experimental and numerical studies on wall-bounded turbulent drag-reducing flows, the underlying physical mechanism of DR remains poorly understood. This is not surprising, since the problem itself is twofold, including two poorly understood problems: turbulence and additives dynamics. In the wall-bounded turbulent flows, the inhomogeneous nature makes it difficult to analyse the interaction between turbulence and polymer microstructures, due to the multitude of competing effects. In contrast, by removing the inhomogeneity emerging from the wall, such as for homogeneous isotropic turbulence (HIT) or bulk turbulence, it is easier to isolate and study the interactions between turbulence and polymer microstructures. Therefore, studies of this kind of turbulence with drag-reducing additives have fundamental importance towards understanding the physics of additives–turbulence interactions. So far, several studies have been carried out based on HIT or bulk turbulence in dilute polymer or surfactant solution through experimental, theoretical and numerical methods and a preliminary understanding of the flow characteristics has been obtained.

To remove the inhomogeneity generated by the wall, the experiments were carried out on grid-generated turbulence or bulk turbulence in drag-reducing fluids. It was found that in grid-generated turbulence in dilute polymer solution, there is a significant alteration of turbulent kinetic energy distribution among scales (Fabula 1966; McComb, Allan & Greated 1977) and energy budget (Friehe & Schwarz 1970) compared with pure water flow and the overall turbulent intensity and pressure drop decrease (Friehe & Schwarz 1970). With the presence of polymers, the flow gives rise to a smaller dissipation rate than that expected for a corresponding Newtonian fluid flow (Van Doorn, White & Sreenivasan 1999). Besides, by flow visualization a suppression of small-scale structures was also obtained which is attributed to an elastic absorption of energy on those scales, and finally results in a truncation of energy cascade (Barnard & Sellin 1969; Van Doorn *et al.* 1999). The above experimental studies of grid turbulence in a dilute polymer solution suggested that DR also exists even in situations where the wall plays no apparent role. Except for grid-generated turbulence, DR was also found in bulk turbulence generated between several counter-rotating disks, using a smooth forcing (Cadot, Bonn & Douady 1998; Bonn *et al.* 2005; Drappier *et al.* 2006; Liberzon *et al.* 2005, 2006). Similarly, a significant decrease in the Lagrangian acceleration variance and a modification of the Eulerian structure function in a dilute polymer solution also indicated the suppression of viscous dissipation and modification of the turbulent energy cascade (Crawford *et al.* 2008; Ouellette, Xu & Bodenschatz 2009).

Based on the experimental results of grid turbulence in a drag-reducing polymer solution, Tabor & De Gennes (1986) and De Gennes (1986) proposed an elastic theory for DR and provided an alternative explanation for the drag-reducing

effect in HIT based on the idea that polymers in turbulent flow exhibit elastic properties even at very low concentrations. They argued that the viscous effects which play a crucial role in Lumley's theory (Lumley 1973) are not at all relevant to the phenomenon of DR. In the theory, two scales are defined for a dilute polymer solution in HIT. (i) $r*$ the trapping length, indicating the scale of the turbulence at which stretching of polymers begins; it is independent of polymer concentration, but dependent on both the relaxation time of polymers and turbulent kinetic dissipation rate. (ii) $r**$ the scale at which the polymer elastic energy is comparable to the turbulent kinetic energy of that scale. They concluded that polymers truncate the classical cascade when $r**$ becomes larger than the usual Kolmogorov scale.

Recently, with the development of numerical simulation many researchers have carried out DNS for forced HIT (FHIT) and decaying HIT (DHIT) to study the additives–turbulence interaction and physical mechanism of DR. In FHIT with the presence of polymers, the energy cascade is deeply altered, i.e. a substantial part of the energy income does not follow the classical Kolmogorov cascade towards viscous dissipation. Instead, it is moved to the microstructures to feed an additional cascade (De Angelis *et al.* 2002*b*, 2005; Vaithianathan & Collins 2003; Jin 2007). A new component in the energy flux is introduced according to the Kármán–Howarth equation (De Angelis *et al.* 2002*b*, 2005) and the turbulent kinetic energy spectra at intermediate scales is reduced, while at high wavenumbers it is increased with the presence of polymers (Vaithianathan & Collins 2003). However, the DNS results of Berti *et al.* (2006) suggested that polymers only partially suppress the turbulent cascade below the Lumley scale, and the velocity at large scales is found to be unaffected and small-scale statistics, such as acceleration, display features typical of Newtonian fluid turbulence. In DHIT with polymer additives, a remarkable alteration of the turbulent kinetic energy spectrum similar to that in FHIT (Vaithianathan & Collins 2003) appeared, and was interpreted based on the effective scale-dependent viscosity (Perlekar, Mitra & Pandit 2006). Moreover, numerical simulation results showed that both the energy dissipation rate and intermittency in the dissipation range are reduced compared to its Newtonian fluid counterpart, and small-scale structures are suppressed (Kalelkar, Govindarajan & Pandit 2005; Perlekar *et al.* 2006). Based on the decrease in energy dissipation rate, Kalelkar *et al.* (2005) proposed a definition of DR rate and found that DR rate increases with the polymer concentration, but decreases with Weissenberg number, inconsistent with that in turbulent channel flow. In a nutshell, the above numerical simulation results also show DR exists in HIT, and the important turbulence parameters change remarkably due to the addition of polymers which are qualitatively consistent with experimental results.

These important previous studies were mainly focused on the DR phenomenon and the characteristics of HIT with polymer additives. However, how the flow structures interact with polymer microstructures has still not been investigated in detail. This is the motivation of our study. As is known, the enstrophy (the strength of the vortex structures) and the strain (directly corresponding to energy dissipation rate) are suitable for describing vortex dynamics and strongly related to energy cascades, and their generation is considered as the impetus of flow maintenance. To explore how the flow is influenced by drag-reducing polymer additives and how polymers contact with flow structures, we carried out DNS of low-Reynolds-number DHIT in a dilute polymer solution and studied the DR mechanism not only through analysing the turbulent-kinetic-energy equation, but also for the first time through analysing the enstrophy and strain transport equations.

2. Governing equations and numerical details

In order to study the additives–turbulence interaction by DNS, an additional polymer stress term to Navier–Stokes equation should be included. There are two major difficulties in the DNS of polymer solution flow: (i) how to model polymers accurately and efficiently; (ii) how to simulate the equation without incurring numerical instabilities. There have been some important conformation models, such as the Oldroyd-B, FENE-P and Giesekus models used in turbulent drag-reducing channel-flow simulations (Sureshkumar & Beris 1995; Dimitropoulos *et al.* 1998; De Angelis *et al.* 2002*a*). Among these models, FENE-P is the most widely used due to its relatively accurate representation of polymers dynamics, minimal computational complexity and its ability to show the drag-reducing behaviour of dilute polymer solution in wall-bounded flows analogous to the experimental results (Sureshkumar *et al.* 1997; De Angelis *et al.* 2002*a*). Therefore, FENE-P is also adopted in our simulation. However, due to the hyperbolic nature of constitutive models it is easy to generate Hadamard instabilities and cause divergence in numerical simulations (Dupret & Marchal 1986). Most studies have solved this problem based on adding an artificial diffusion term (Sureshkumar & Beris 1995), continuous decomposition (Vaithianathan & Collins 2003) or Cholesky decomposition (Vaithianathan & Collins 2003) and a high-order discrete scheme for conformation equations such as the MINMOD scheme (Yu & Kawaguchi 2004). Vaithianathan *et al.* (2006) discussed the remaining questions of the above methods and proposed the Kurganov–Tadmor (KT) scheme to solve the Hadamard instabilities. The scheme is second-order accurate in space everywhere except for the grid points losing symmetric positive definite (SPD) property. Where it occurs the scheme automatically becomes first-order accurate for these points to maintain the SPD property. To guarantee the SPD property of the conformation tensor at all times and all points, the KT scheme was used in our numerical simulations.

The governing equations for dilute polymer solutions in DHIT are

$$\frac{\partial \boldsymbol{u}}{\partial t} + \boldsymbol{u} \cdot \nabla \boldsymbol{u} = -\frac{1}{\rho} \nabla p + \frac{1}{\rho} \nabla \cdot \boldsymbol{T}^{[s]} + \frac{1}{\rho} \nabla \cdot \boldsymbol{T}^{[p]}, \tag{2.1}$$

$$\frac{\partial \boldsymbol{C}}{\partial t} + \boldsymbol{u} \cdot \nabla \boldsymbol{C} = \boldsymbol{C} \cdot \nabla \boldsymbol{u} + \nabla \boldsymbol{u}^{\mathrm{T}} \cdot \boldsymbol{C} - \frac{f(r)\boldsymbol{C} - \boldsymbol{I}}{\tau_p}. \tag{2.2}$$

where $\boldsymbol{u}(\boldsymbol{x}, t)$ is the velocity vector, p is the local pressure, ρ is the fluid density, $\boldsymbol{T}^{[s]} = 2\rho \nu^{[s]} \boldsymbol{S}$ is the Newtonian stress tensor due to the solvent, $\nu^{[s]}$ is the solvent kinetic viscosity and $\boldsymbol{S} = (\Gamma_{ij} + \Gamma_{ji})/2$ is the rate of strain tensor, $\nabla \boldsymbol{u} = \Gamma_{ij} = \partial u_i / \partial x_j$ and $\nabla \boldsymbol{u}^{\mathrm{T}} = \Gamma_{ji} = \partial u_j / \partial x_i$, $\boldsymbol{T}^{[p]} = (\rho \nu^{[p]} / \tau_p)(f(r)\boldsymbol{C} - \boldsymbol{I})$ is the additional elastic stress tensor due to polymers, $\nu^{[p]}$ is the polymer viscosity and $\boldsymbol{I}$ is the unit tensor, τ_p is the polymer-relaxation time, $\boldsymbol{C}$ is the polymer conformation tensor. In the FENE-P model, $f(r) = (L^2 - 3)/(L^2 - r^2)$ ensures the finite extensibility, $r = \sqrt{\mathrm{trace}(\boldsymbol{C})}$ and L are the extension length and the maximum possible extension of polymers, respectively.

To solve (2.1), a standard pseudo-spectral code with 96^3 collocation points in the periodic cubic domain of size $\mathbb{L} = 2\pi$ cm is used for spatial discretization (Rogallo 1981; Canuto *et al.* 1988). Note that in the simulations the spatial resolution is sufficient to capture the information at the smallest scale, i.e. the Kolmogorov scale. Our low-resolution results are similar to the high-resolution results of Perlekar *et al.* (2006), and a second-order Adams–Bashforth scheme is adopted for time marching with all the nonlinear terms fully de-aliased by the 3/2 rule. The spectral and high-order compact schemes are not suitable for solving (2.2), as they lose spectral

convergence in the vicinity of the discontinuities (Vaithianathan *et al.* 2006). Therefore, in our simulations for (2.2), the finite difference method is used. For time marching, a second-order Adams–Bashforth scheme is adopted. In spatial domain, we use a second-order central difference scheme except for the convective term. For the convective term in (2.2), a second-order KT scheme is used, and it can be discretized as follows (Vaithianathan *et al.* 2006):

$$
\boldsymbol{u} \cdot \nabla \boldsymbol{C} = \frac{H_{i+1/2,j,k}^x - H_{i-1/2,j,k}^x}{\Delta x} + \frac{H_{i,j+1/2,k}^y - H_{i,j-1/2,k}^y}{\Delta y} + \frac{H_{i,j,k+1/2}^z - H_{i,j,k-1/2}^z}{\Delta z},
$$

(2.3)

where the convective flux in each direction is given by

$$
\left.\begin{aligned}
H_{i+1/2,j,k}^x &= \tfrac{1}{2} u_{i+1/2,j,k}(\boldsymbol{C}_{i+1/2,j,k}^+ + \boldsymbol{C}_{i+1/2,j,k}^-) - \tfrac{1}{2} |u_{i+1/2,j,k}|(\boldsymbol{C}_{i+1/2,j,k}^+ - \boldsymbol{C}_{i+1/2,j,k}^-), \\
H_{i,j+1/2,k}^y &= \tfrac{1}{2} v_{i,j+1/2,k}(\boldsymbol{C}_{i,j+1/2,k}^+ + \boldsymbol{C}_{i,j+1/2,k}^-) - \tfrac{1}{2} |v_{i,j+1/2,k}|(\boldsymbol{C}_{i,j+1/2,k}^+ - \boldsymbol{C}_{i,j+1/2,k}^-), \\
H_{i,j,k+1/2}^z &= \tfrac{1}{2} w_{i,j,k+1/2}(\boldsymbol{C}_{i,j,k+1/2}^+ + \boldsymbol{C}_{i,j,k+1/2}^-) - \tfrac{1}{2} |w_{i,j,k+1/2}|(\boldsymbol{C}_{i,j,k+1/2}^+ - \boldsymbol{C}_{i,j,k+1/2}^-).
\end{aligned}\right\}
$$

(2.4)

The superscripts '+' and '−' on the right-hand side in (2.4) designate values of the conformation tensor at the interface obtained in the limit approaching the point of interest from the right (+) or left (−) side. The conformation tensor $\boldsymbol{C}$ at the interface is constructed from the following second-order, piecewise, linear approximations:

$$
\left.\begin{aligned}
\boldsymbol{C}_{i+1/2,j,k}^\pm &= \boldsymbol{C}_{i+1/2\pm1/2,j,k} \mp \left(\frac{\Delta x}{2}\right)\left(\frac{\partial \boldsymbol{C}}{\partial x}\right)_{i+1/2\pm1/2,j,k}, \\
\boldsymbol{C}_{i,j+1/2,k}^\pm &= \boldsymbol{C}_{i,j+1/2\pm1/2,k} \mp \left(\frac{\Delta y}{2}\right)\left(\frac{\partial \boldsymbol{C}}{\partial y}\right)_{i,j+1/2\pm1/2,k}, \\
\boldsymbol{C}_{i,j,k+1/2}^\pm &= \boldsymbol{C}_{i,j,k+1/2\pm1/2} \mp \left(\frac{\Delta z}{2}\right)\left(\frac{\partial \boldsymbol{C}}{\partial z}\right)_{i,j,k+1/2\pm1/2}.
\end{aligned}\right\}
$$

(2.5)

Here, potential candidates for approximating the gradients are

$$
\left(\frac{\partial \boldsymbol{C}}{\partial x}\right)_{i,j,k} = \begin{cases} (\boldsymbol{C}_{i+1,j,k} - \boldsymbol{C}_{i,j,k})/\Delta x, \\ (\boldsymbol{C}_{i,j,k} - \boldsymbol{C}_{i-1,j,k})/\Delta x, \\ (\boldsymbol{C}_{i+1,j,k} - \boldsymbol{C}_{i-1,j,k})/(2\Delta x). \end{cases}
$$

(2.6)

We selected a derivative approximation that can yield SPD results for $\boldsymbol{C}_{i-1/2}^+$ and $\boldsymbol{C}_{i+1/2}^-$. When two or more candidates satisfy the criterion, we select the one which maximizes the minimum eigenvalue for these two tensors. When none of them meet this criterion, the derivative is set to zero, reducing to first-order accurate. The finite-volume update for $\boldsymbol{C}$ requires the area-averaged velocities at the edge of the volume surrounding each grid point. The following method is used (Vaithianathan *et al.* 2006):

$$
\left.\begin{aligned}
u_{i\pm1/2,j,k} &= F^{-1}\left\{ \hat{u} \mathrm{e}^{\pm \mathrm{i} k_x \Delta x/2} \frac{\sin(k_y \Delta y/2)}{k_y \Delta y/2} \frac{\sin(k_z \Delta z/2)}{k_z \Delta z/2} \right\}, \\
v_{i,j\pm1/2,k} &= F^{-1}\left\{ \hat{v} \mathrm{e}^{\pm \mathrm{i} k_y \Delta y/2} \frac{\sin(k_z \Delta z/2)}{k_z \Delta z/2} \frac{\sin(k_x \Delta x/2)}{k_x \Delta x/2} \right\}, \\
w_{i,j,k\pm1/2} &= F^{-1}\left\{ \hat{w} \mathrm{e}^{\pm \mathrm{i} k_z \Delta z/2} \frac{\sin(k_x \Delta x/2)}{k_x \Delta x/2} \frac{\sin(k_y \Delta y/2)}{k_y \Delta y/2} \right\},
\end{aligned}\right\}
$$

(2.7)

Cases	δt(s)	L	$\nu^{[s]}$(cm^2 s^{-1})	τ_p(s)	β
Run 96-A	1.0×10^{-3}	100	10^{-2}	0.1	0.6,0.7,0.8,0.9
Run 96-B	1.0×10^{-3}	100	10^{-2}	0.15	0.6,0.7,0.8,0.9
Run 96-C	1.0×10^{-3}	100	10^{-2}	0.2	0.6,0.7,0.8,0.9
Run 96-D	1.0×10^{-3}	100	10^{-2}	0.08,0.12,0.18	0.6
Run 96-E	1.0×10^{-3}	0	10^{-2}	0	1

TABLE 1. The parameters δt, L, $\nu^{[s]}$, τ_p and β for our runs. Run 96-A, $Re_\lambda = 26.2$, $Wi = 0.62$; Run 96-B, $Re_\lambda = 26.2$, $Wi = 0.93$; Run 96-C, $Re_\lambda = 26.2$, $Wi = 1.24$; Run 96-D, $Re_\lambda = 26.2$, $Wi = 0.50, 0.74, 1.11$; Run 96-E, $Re_\lambda = 26.2$, $Wi = 0$, Newtonian fluid case. We use $\rho = 1$ g cm^{-3} for all simulations. $\beta = \nu^{[s]}/(\nu^{[s]} + \nu^{[p]})$ is a dimensionless measure of dilute polymer solution concentration, and smaller β corresponds to denser polymer solution.

where $u_{i\pm1/2,j,k}$, $v_{i,j\pm1/2,k}$ and $w_{i,j,k\pm1/2}$ are the area-averaged velocities at the edge of the volume surrounding each grid point; $\hat{u}(k_x, k_y, k_z)$, $\hat{v}(k_x, k_y, k_z)$ and $\hat{w}(k_x, k_y, k_z)$ are the Fourier coefficients of velocities at each grid point. Hereafter variables with hats '^' are in Fourier space.

Simulations are based on the divergence-free initial velocity field $\hat{\boldsymbol{u}}_0(\boldsymbol{k})$, i.e. $\nabla \cdot \hat{\boldsymbol{u}}_0(\boldsymbol{k}) = 0$, which is generated in Fourier space according to Rogallo's procedure (Rogallo 1981)

$$\hat{\boldsymbol{u}}_0(\boldsymbol{k}) = \frac{\alpha(\boldsymbol{k})kk_2 + \beta(\boldsymbol{k})k_1k_3}{k\sqrt{k_1^2 + k_2^2}}\boldsymbol{e}_1 + \frac{\beta(\boldsymbol{k})k_2k_3 - \alpha(\boldsymbol{k})kk_1}{k\sqrt{k_1^2 + k_2^2}}\boldsymbol{e}_2 - \frac{\beta(\boldsymbol{k})(k_1^2 + k_2^2)}{k_2^2}\boldsymbol{e}_3, \quad (2.8)$$

where $\alpha(\boldsymbol{k}) = \sqrt{(E_0(k)/4\pi k^2)}e^{i\theta_1}\cos\phi$, $\beta(\boldsymbol{k}) = \sqrt{(E_0(k)/4\pi k^2)}e^{i\theta_2}\sin\phi$, θ_1, θ_2 and ϕ are uniform random variables between 0 and 2π; $\boldsymbol{e}_1$, $\boldsymbol{e}_2$ and $\boldsymbol{e}_3$ are the unit vectors along the three axes in $\boldsymbol{k}$ space; $\boldsymbol{k}$ is the wave vector with component $k_m = (-N/2, \ldots, -1, 0, 1, \ldots, N/2 - 1)$, $k = |\boldsymbol{k}|$, and initial energy spectrum $E_0(k) = 0.01k^4 e^{-0.14k^2}$. For the initial conformation field, polymers were assumed non-stretched, corresponding to $C_{ij}^0(\boldsymbol{x}) = \delta_{ij}$ (Vaithianathan & Collins 2003; Perlekar *et al.* 2006).

In Fourier space, the turbulent kinetic energy spectra $E(k, t) = (1/2) \Sigma_{k-1/2 < k' \leqslant k+1/2}|\boldsymbol{u}(\boldsymbol{k}, t)|^2$; the total turbulent kinetic energy in Fourier space $\xi(t) = \Sigma_k E(k, t)$ and in physical space $\xi(t) = \int_{\mathbb{L}^3} 1/2 u_i^2(\boldsymbol{x}, t)\,dV$; the energy dissipation rate in Fourier space $\varepsilon(t) = \nu^{[s]}\Sigma_k k^2 E(k, t)$ and in physical space $\varepsilon(t) = \int_{\mathbb{L}^3} \nu^{[s]}\Gamma_{ij}^2\,dV$. The Taylor-scale Reynolds number, Re_λ, and the Weissenberg number, Wi, are defined as $Re_\lambda = \sqrt{20}\xi_m^{[N]}/\sqrt{3\nu^{[s]}\varepsilon_m^{[N]}}$, $Wi = \tau_p\sqrt{\varepsilon_m^{[N]}/\nu^{[s]}}$, respectively, where $\xi_m^{[N]}$ and $\varepsilon_m^{[N]}$ are at $t = t_m$ in Fourier space; here, t_m corresponds to the moment at which $\varepsilon^{[N]}$ reaches to its maximum amplitude; the superscript 'N' represents the Newtonian fluid case (Perlekar *et al.* 2006). The parameters for all simulations are shown in table 1.

3. Results and discussions

3.1. *Some characteristics of decaying homogeneous isotropic turbulence*

In our numerical simulations, we firstly confirmed that $\langle u^2 \rangle \approx \langle v^2 \rangle \approx \langle w^2 \rangle$ and $\langle uv \rangle \approx \langle uw \rangle \approx \langle vw \rangle \approx 0$, which is an indication of isotropic turbulence characteristics of DHIT for Newtonian fluid and polymer solution cases. One of the most meaningful parameters in DHIT is the Taylor microscale $\lambda = \sqrt{15\nu\xi/\varepsilon}$, as shown in figure 1. λ decreases at first and then grows quickly, which implies the development of small-scale structures occurring in the energy propagation period (EPP) and the decay of
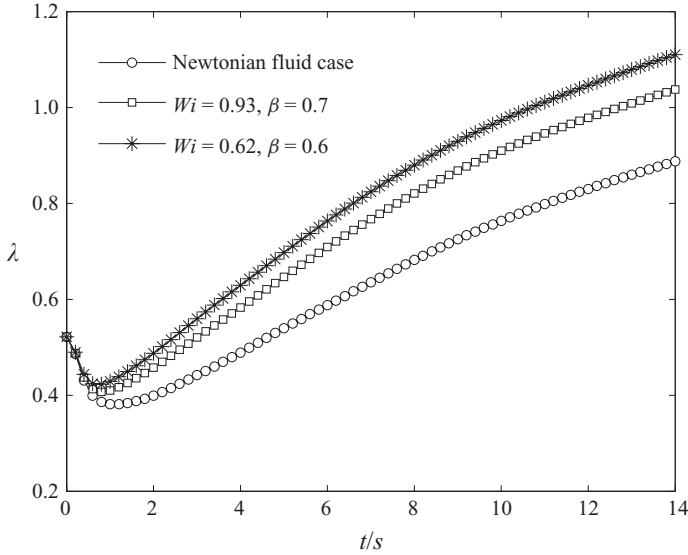
FIGURE 1. Temporal evolution of Taylor microscales, λ, in DHIT for Newtonian fluid and polymer solution cases.

small-scale structures in the energy decay period (EDP) (Kraichnan 1964; Meng 2004). Further, in EPP $\lambda^{[p]} \approx \lambda^{[N]}$ (hereinafter, the superscripts 'p' represent the polymer solution case) and in EDP $\lambda^{[p]} > \lambda^{[N]}$, suggesting that the decay of small-scale structures in the polymer solution case is faster than that in the Newtonian fluid case, i.e. an inhibition of turbulent motions at small scales. It can be regarded as the polymer's effect on flow structures and an origin of DR. Later we will discuss drag-reducing effects in detail from other viewpoints.

Next, we will analyse the energy budget of DHIT in both the Newtonian fluid and polymer solution cases. In the Newtonian fluid case, there is no external forcing and no mean shear, but only viscous dissipation, so we can obtain the turbulent kinetic energy budget equation as follows:

$$\frac{\mathrm{d}\xi^{[N]}}{\mathrm{d}t} = -\varepsilon^{[N]}. \tag{3.1}$$

In the polymer solution case, however, it is different from that in the Newtonian fluid case due to the effect of polymer elastic stress, as follows (Jin 2007):

$$\frac{\mathrm{d}\xi^{[p]}}{\mathrm{d}t} = -\varepsilon^{[p]} - G, \tag{3.2}$$

where G represents energy transfer between flow structures and polymer microstructures; in physical space $G = \int_{\mathbb{L}^3} \Gamma_{ij} T_{ij}^{[p]} \, \mathrm{d}V$ and in Fourier space $G = \Sigma_k \mathrm{Im}(k) = \Sigma_k (\hat{\Gamma}_{ij} (\hat{T}_{ij}^{[p]})^* + (\hat{\Gamma}_{ij})^* \hat{T}_{ij}^{[p]})$, where $()^*$ indicates the complex conjugate and $\mathrm{Im}(k)$ is the energy transfer spectrum at wavenumber k. $G > 0$ implies energy transfer from flow structures to polymer microstructures and $G < 0$ implies the contrary energy transfer process. Because of its flexibility, polymers can absorb energy from flow structures to store it as the polymer elastic energy and dissipate it by elasticity. So another equation is used to show this relationship, which is as follows
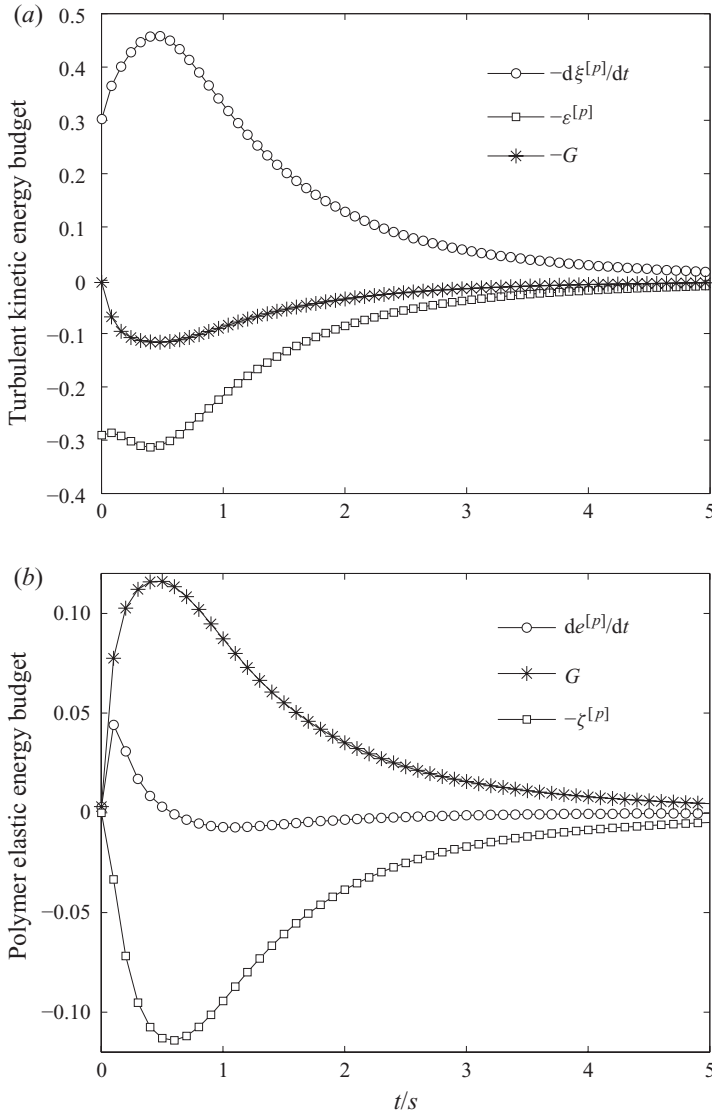
FIGURE 2. Energy budget in DHIT of polymer solution in physical space, $Wi = 0.62$, $\beta = 0.7$. (*a*) energy budget based on (3.2); (*b*) energy budget based on (3.3).

(Jin 2007):

$$\frac{\mathrm{d}e^{[p]}}{\mathrm{d}t} = G - \zeta^{[p]}, \tag{3.3}$$

where $e^{[p]}$ is the polymer elastic energy in physical space given by $e^{[p]} = \int_{\mathbb{L}^3}(\nu^{[p]}L^2/2\tau_p)\log f(r)\,\mathrm{d}V$, and $\zeta^{[p]}$ is the polymer elastic dissipation rate in physical space given by $\zeta^{[p]} = \int_{\mathbb{L}^3} f(r)T_{ii}^{[p]}/(2\tau_p)\,\mathrm{d}V$. The energy budget in the polymer solution case is shown in figure 2. In EPP, due to the development of small-scale structures polymers shift from the equilibrium to a stretched state and absorb a part of the turbulent kinetic energy (De Angelis *et al.* 2005). In EDP, due to the decrease in motions at all scales, polymers can not be stretched as much as in EPP so that polymers may release a part of the elastic energy and absorb less energy from flow
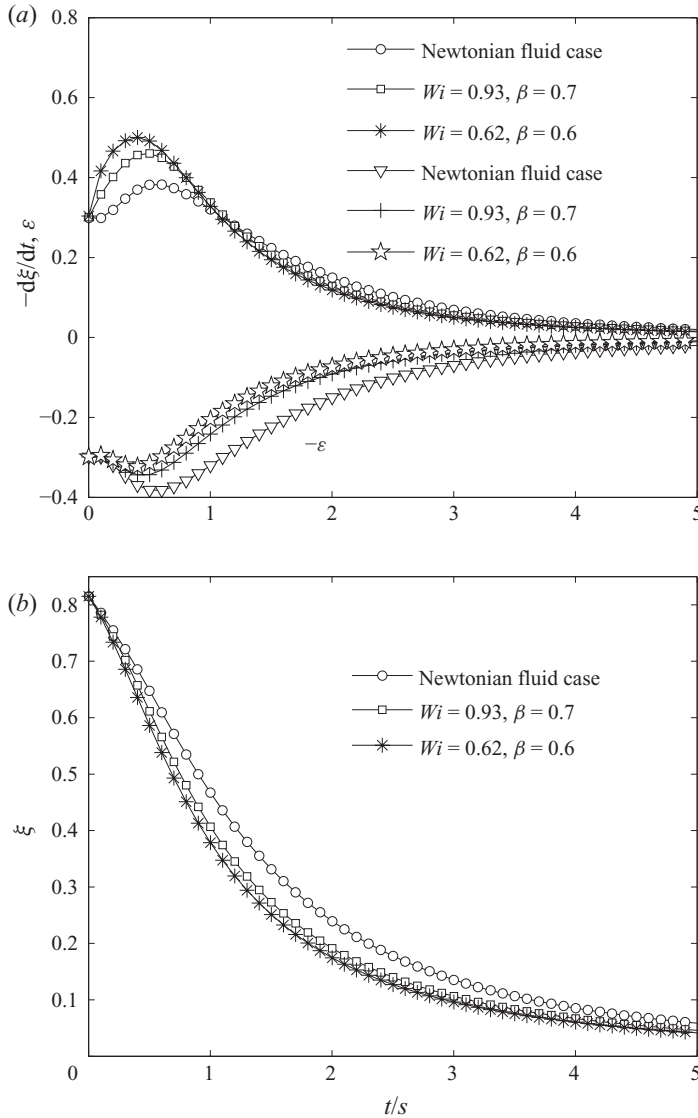
FIGURE 3. Temporal evolution of (*a*) decay rate of the turbulent kinetic energy ($d\xi/dt$), energy dissipation rate (ε) and (*b*) the total turbulent kinetic energy (ξ).

structures. In any case the results show that polymers always absorb the turbulent kinetic energy ($G > 0$) from flow structures during all the periods, leading to weaker remaining turbulent kinetic energy.

In DHIT, the initial energy is the initial turbulent kinetic energy, and the larger decay rate of the turbulent kinetic energy represents a more marked inhibition of turbulence and a stronger tendency to make flow regular, analogous to the drag-reducing effect in wall-bounded turbulent flows. In figure 3, we show the temporal evolution of $d\xi/dt$, ε and ξ in the Newtonian fluid and polymer solution cases, respectively. From (3.1), we can see that in the Newtonian fluid case the unique dissipative mode is due to viscosity; however, in polymer solution case, there exist two modes due to viscosity and elasticity, respectively. The decay processes in the two

cases experience both the periods (EPP and EDP), but it presents a larger decay rate during the whole EPP and the early stage of EDP, and a smaller decay rate during the later stage of EDP in the polymer solution case, as shown in figure 3(*a*). And according to the rapid decay in the former period, the decay of the turbulent kinetic energy is eventually much faster in the polymer solution case, indicating that DR occurs in DHIT with polymer additives without a solid boundary layer. However, this is inconsistent with the numerical results of Vaithianathan & Collins (2003) in which the decay rate of the turbulent kinetic energy is smaller than that in the Newtonian fluid case due to the non-zero of the initial conformation field or the non-zero elastic energy. Further, figure 3(*a*) clearly shows that, due to the energy-absorption effect of polymers, the viscous dissipation rate in the polymer solution case is smaller. The decrease of energy dissipation rate corresponding to the nonlinearity of turbulence further proves the existence of the DR effect from another point.

According to the above analysis, it is known that DR is directly related to the decay rate of turbulent kinetic energy. Hence, through examining the decaying process in DHIT for the polymer solution case, we propose an intuitive and natural definition for the DR rate occurring in DHIT based on the statistical kinetic energy decay, different from that in Kalelkar *et al.* (2005) and Perlekar *et al.* (2006) based on the energy dissipation rate, as follows:

$$
DR(\%) = \frac{\displaystyle\int_0^{t_m} (\mathrm{d}\xi/\mathrm{d}t)^{[p]}\,\mathrm{d}t - \int_0^{t_m} (\mathrm{d}\xi/\mathrm{d}t)^{[N]}\,\mathrm{d}t}{\displaystyle\int_0^{t_m} (\mathrm{d}\xi/\mathrm{d}t)^{[N]}\,\mathrm{d}t} \times 100\,\% = \frac{\Delta\xi_m^{[p]} - \Delta\xi_m^{[N]}}{\Delta\xi_m^{[N]}} \times 100\,\%,
$$

(3.4)

where t_m is the time when the Newtonian dissipation rate reaches its maximum and $\Delta\xi_m^{[N]}$ and $\Delta\xi_m^{[p]}$ are the decrease of turbulent kinetic energy from $t=0$ to $t=t_m$ in the Newtonian fluid case and polymer solution case, respectively. As for the definition of DR based on dissipation rate in Kalelkar *et al.* (2005) and Perlekar *et al.* (2006), a smaller dissipation rate compared with that of the Newtonian fluid is the outcome of DR, so the definition is from the resultant viewpoint.

As an example, DR versus β is plotted in figure 4 for $Wi = 0.93$, showing that DR decreases with β (i.e. DR increases with the polymer concentration). In the inset of figure 4, the relation between DR and Wi shows DR decreases with Wi, unlike in the turbulent channel flow, but qualitatively consistent with the results of Perlekar *et al.* (2006). We also investigate the temporal evolution of mean relative conformation rate with different concentrations, as shown in figure 5. It shows that during the EDP the mean relative extension decreases with the polymer concentration and is almost the same during the EPP. The reason is that for larger concentration more marked DR occurs, and at the same time the mean velocity gradient generated by turbulent fluctuations weakens, leading to a smaller polymer extension.

3.2. *Spectral analysis in DHIT*

For the classical turbulent energy cascade in the Newtonian fluid turbulent flow, larger-scale structures transfer the turbulent kinetic energy into smaller-scale structures until the smallest scale (dissipative scale), where the energy is exhausted as heat loss due to viscosity. To investigate the multiscale interaction between flow structures and polymer microstructures, we pay attention to the $E(k)$ and $Im(k)$ in Fourier space. The temporal evolution of $E(k)$ in the Newtonian fluid and polymer solution cases are shown in figures 6(*a*) and 6(*b*), respectively. During the EPP, nonlinear energy
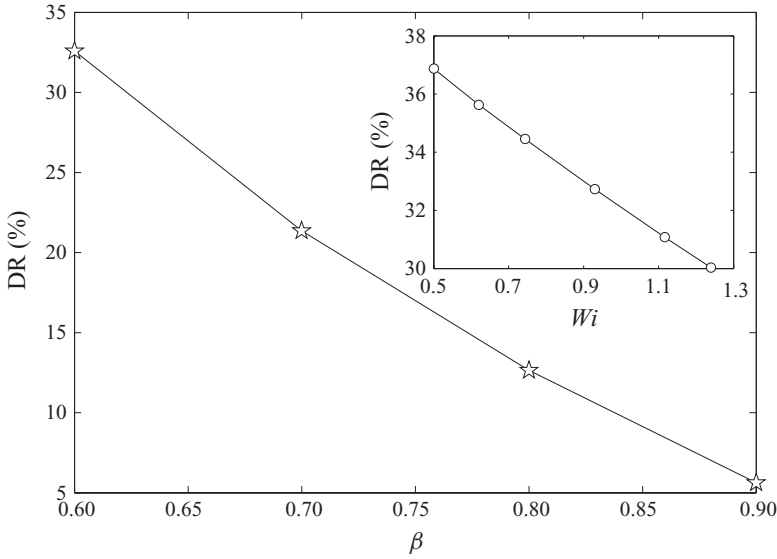
FIGURE 4. DR rate versus β in DHIT with polymer additives, $Wi = 0.93$. Inset: DR rate versus Wi, $\beta = 0.6$.
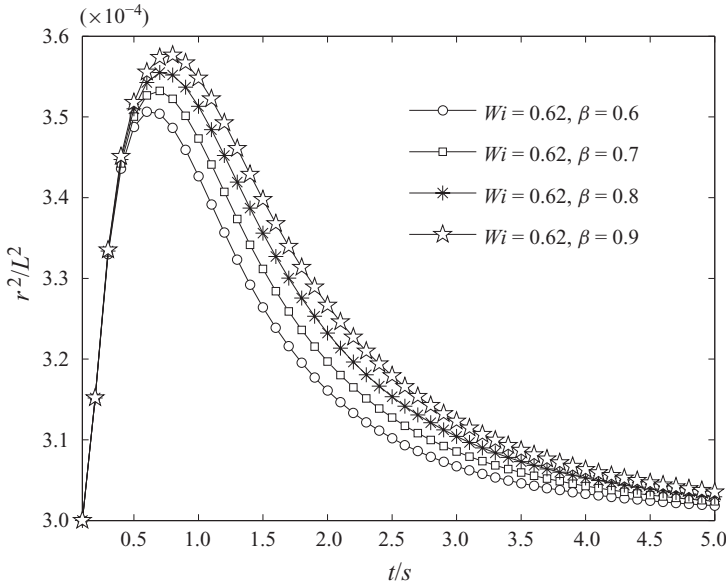

FIGURE 5. The time evolution of r^2/L^2 for different concentrations.

transfer dominates and the energy is transferred from small wavenumbers to large wavenumbers so as to raise the tail of energy spectra, but during the EDP, the viscous effect dominates so that the dissipation always lowers the tail of energy spectra. However, $E^{[p]}(k)$ is apparently different from $E^{[N]}(k)$, especially in the EDP, where $E^{[p]}(k) < E^{[N]}(k)$ at large and intermediate scales and $E^{[p]}(k) \gg E^{[N]}(k)$ at small scales, as shown in figure 6(*b*). Besides, $E^{[p]}(k)$ keeps nearly constant at some scales range,
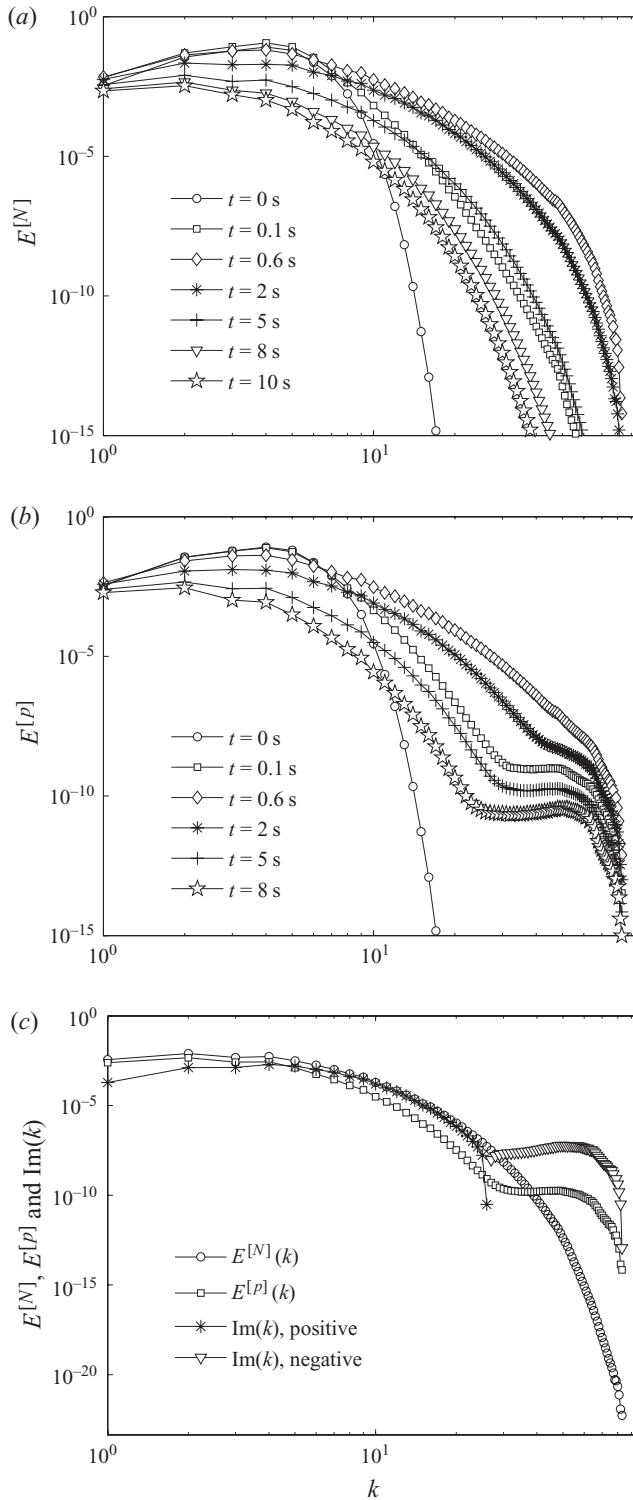
FIGURE 6. Turbulent-kinetic-energy spectra $E(k)$ in DHIT. (*a*) Newtonian fluid case; (*b*) polymer solution case, $Wi = 0.62$, $\beta = 0.7$; (*c*) $E(k)$ for Newtonian fluid case and $E(k)$ and Im(k) for polymer solution case, $Wi = 0.62$, $\beta = 0.7$ at $t = 5.0$ s.
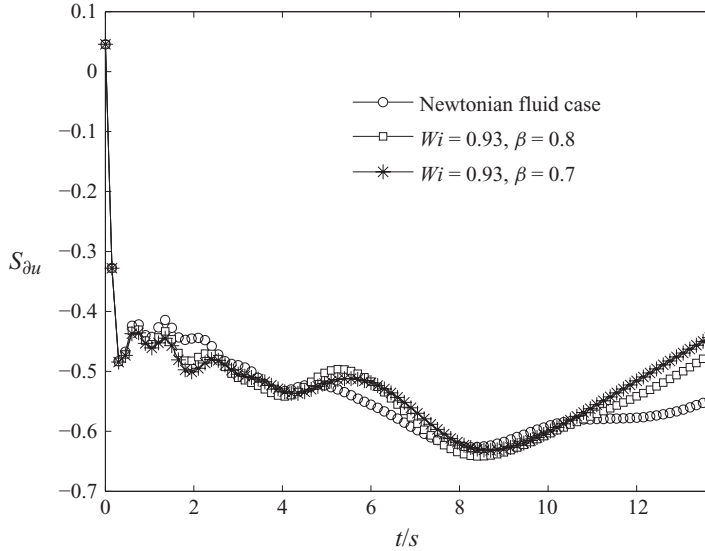
FIGURE 7. The evolution of $S_{\partial u}$ in DHIT of Newtonian fluid and polymer solutions.

i.e. the polymer dominant scale range, and this range becomes wider with advancing time, straightforwardly indicating that the turbulent kinetic energy transfer process for the Newtonian fluid flow which has been modified in DHIT with polymer additives is consistent with the experimental result of Fabula (1966) and numerical results of Perlekar *et al.* (2006). To interpret this intriguing phenomenon, $\text{Im}(k)$ is shown in figure 6(*c*). It is found that at large and intermediate scales $\text{Im}(k) > 0$, indicating that polymers absorb turbulent kinetic energy from flow structures to store it as the elastic energy and dissipate it by elasticity; however, at the special polymer dominant scale range ($E^{[p]}(k)$ keeps nearly constant), $\text{Im}(k) < 0$, adequately suggesting that the energy is transferred from polymer microstructures to the small-scale flow structures, resulting in $E^{[p]}(k) \gg E^{[N]}(k)$ at these scales.

In summary, we have obtained that, in DHIT with polymer additives: (i) polymers absorb the turbulent kinetic energy from large and intermediate scales flow structures; (ii) at large and intermediate scales, the turbulent kinetic energy transfer process is partly similar to the classical Kolmogorov energy cascade; (iii) when it comes to the polymer-dominant-scale range, the energy cascade is modified, i.e. part of the energy is transferred from the polymer microstructures into the flow structures of this range to make the turbulent kinetic energy keep nearly constant at this range of scales.

3.3. *Intermittency analysis in DHIT*

The velocity-derivative skewness $S_{\partial u} = -\langle(\partial u/\partial x)^3\rangle/\langle(\partial u/\partial x)^2\rangle^{3/2}$ is a measure of the nonlinearity of Navier–Stokes equation and is directly related to the production of the dissipation rate of the turbulent kinetic energy, or, equivalently, the production of the enstrophy (Mansour & Wray 1994). Figure 7 shows the temporal evolution of $S_{\partial u}$: it drops rapidly at first and then bounces back and varies slowly. The rapid drop corresponds to the development of turbulence in the EPP, and the small variation implies that turbulence remains at some level even in the EDP. Also, in the polymer solution case $S_{\partial u}$ is smaller in amplitude during the later stage of the EDP, representing smaller production of the dissipation rate of the turbulent kinetic energy and weaker nonlinearity of Navier–Stokes equation due to less turbulent
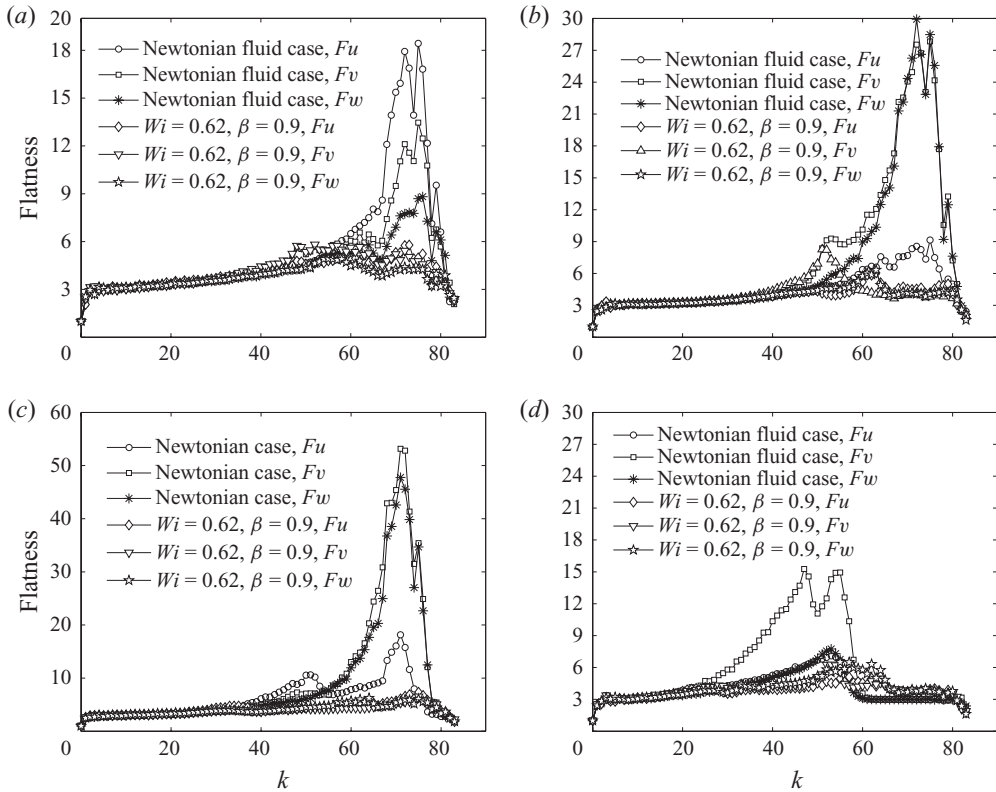
FIGURE 8. Flatness of each velocity component versus wavenumber for DHIT of Newtonian fluid and polymer solutions cases. (*a*) $t = 0.6$ s; (*b*) $t = 2$ s; (*c*) $t = 5$ s and (*d*) $t = 8$ s.

kinetic energy contained compared with that in the Newtonian fluid case (as shown in figure 3*b*). From this viewpoint, the existence of the DR effect by polymer additives can also be demonstrated.

Further, we also explore the multiscale property of flatness (or kurtosis) $F_{u_i} = (\langle \hat{u}_i^4 \rangle_k)/(\langle \hat{u}_i^2 \rangle_k^2)$, in DHIT for both cases (here $\hat{u}_i$ represents the velocity in Fourier space at each scale, and k is the wavenumber), as shown in figure 8. For the two cases, turbulence structures at small scales display stronger intermittency with a peak value of F_{u_i} and at large scales are almost non-intermittent. With time evolution, the strong intermittent scale range moves towards large scales and the intermittency at small scales nearly disappears. Comparing these two cases, we can find that the intermittency for large-scale flow structures in polymer solution case is almost unaltered, but suppressed for small-scale flow structures. But in the later EDP (figure 8*d* at $t = 8$ s), the small-scale flow structures in the polymer solution case behave more intermittently than that in the Newtonian fluid case.

3.4. *Enstrophy, vortex structures and strain in decaying homogeneous isotropic turbulence*

The existence of coherent or quasi-ordered structures in turbulent flow fields has been known since the direct observation of these structures in numerically simulated stationary HIT by Siggia (1986) and experimental observation by Douady, Couder & Brachet (1991). Coherent structures may be divided roughly into two groups: tube-like and sheet-like vortex structures. Jiménez & Wray (1998) confirmed that the

tube-like vortex structures are the dominant structures of isotropic turbulence at high vorticity amplitudes. Up to now, different mathematics-based (particularly based on the kinematics implied by the velocity-gradient tensor) methods for the identification of the tube-like vortex structures have been introduced, such as (i) the D criterion, based on the complex eigenvalues of the velocity-gradient tensor (Perry & Chong 1987); (ii) the Q criterion, based on the second invariant of the velocity-gradient tensor (Zhong, Huang & Adrian 1998); (iii) the λ_{ci} criterion, based on the imaginary part of the complex eigenvalue pair of the velocity-gradient tensor (Zhou *et al.* 1999); (iv) the λ_2 criterion, based on the analysis of the Hessian tensor of the pressure (Jeong & Hussain 1995). Examining coherent structures of DHIT with and without polymers and investigating their characteristics will help us further to understand the drag-reducing effect of polymers. So, next we will study the influence of polymers on the tube-like vortex structures in DHIT by investigating the characteristics of the enstrophy and strain and visualizing them based on the Q criterion.

The enstrophy indicates the strength of the tube-like vortex structures and mainly generated by the stretch of the tube-like vortex structures, which is regarded as the impetus of flow maintenance. To show the polymer effect, we study the polymer contribution to the enstrophy in DHIT. Based on (2.1), the enstrophy transport equation for DHIT with polymer additives can be deduced as follows:

$$\underbrace{\frac{\partial \langle \Omega \rangle}{\partial t}}_{R_{ens}} = \underbrace{\langle \omega_i S_{ij} \omega_j \rangle}_{S_{ens}} + \underbrace{\left\langle \nu^{[s]} \frac{\omega_i \partial^2 \omega_i}{\partial x_j \partial x_j} \right\rangle}_{V_{ens}} + \underbrace{\left\langle \omega_i \frac{\partial^2 T_{mj}^{[p]}}{\partial x_m \partial x_n} \epsilon_{nji} \right\rangle}_{P_{ens}}, \qquad (3.5)$$

where the operator $\langle \cdot \rangle$ denotes ensemble average; ϵ_{nji} is the permutation symbol; ω_i is the ith component of the vorticity, $\boldsymbol{\omega} = \nabla \times \boldsymbol{u}$ and $\Omega = \omega_i \omega_i / 2$ is the enstrophy; R_{ens} is the increase rate of Ω; S_{ens} is the enstrophy production due to vortex stretching; V_{ens} is the enstrophy dissipation and P_{ens} is the polymer effect, which does not appear in the Newtonian fluid case.

Firstly, the temporal evolution of Ω in both the Newtonian fluid and polymer solution cases, and each term in (3.5), are shown in figures 9(*a*) and 9(*b*), respectively. In the EPP, Ω increases and vortex structures are stretched, indicating the generation of the small-scale vortex structures. In the EDP, Ω and S_{ens} decrease, indicating the suppression and dissipation of the vortex structures. It is consistent with the temporal evolution of the turbulent kinetic energy spectra (showing in the EPP the turbulent kinetic energy of small-scale structures increases and in the EDP the turbulent kinetic energy of all scales decreases, as mentioned previously). In both EPP and EDP, the enstrophy in polymer solution case is remarkably weak compared with its Newtonian counterpart. Besides, figure 9(*b*) shows that $P_{ens} < 0$ and $S_{ens}^{[p]} < S_{ens}^{[N]}$, adequately suggesting the inhibition effect of vortex structures by polymers. To show the influence of polymers on the enstrophy in detail, probability density functions of $s_{ens} = \omega_i S_{ij} \omega_j$ and $p_{ens} = \omega_i (\partial^2 T_{mj}^{[p]} / \partial x_m \partial x_n \epsilon_{nji})$ are calculated and shown in figure 10. The results show that s_{ens} is positively skewed, i.e. it tends to stretch flow vortices. However, $s_{ens}^{[p]}$ is weaker than $s_{ens}^{[N]}$ and p_{ens} is negatively skewed, i.e. the stretch of flow vortices and the growth of enstrophy are inhibited by the polymers. In summary, adding polymer additives to DHIT can reduce the strength of vortex stretching (which is the source and impetus of small-scale turbulence generation) and the growth of the enstrophy, so as to produce the drag-reducing phenomenon.

To make a further intuitive confirmation of the above analysis, we visualize the evolution of the tube-like vortex structures in both the Newtonian fluid and polymer
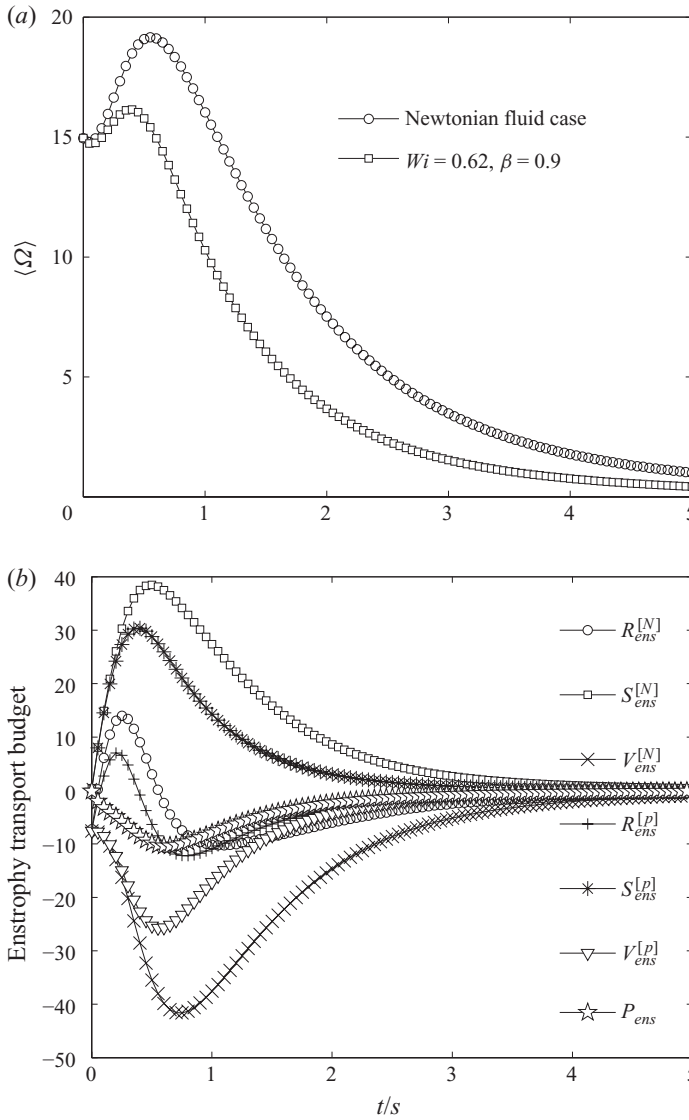
FIGURE 9. Temporal evolution of (*a*) the enstrophy and (*b*) each term in the enstrophy transport (3.5), $Wi = 0.62$, $\beta = 0.6$.

solution cases in EDP, as shown in figure 11. A marked inhibition of small-scale structures in polymer solution case can be observed. With advancing time, the strength of the tube-like vortex structures decreased in EDP, and in polymer solution case, the decrease of the tube-like vortex strength is much faster as compared with its Newtonian fluid counterpart, due to the suppression effect of vortex stretching by polymer additives as discussed above.

Tennekes & Lumley (1972) argued that vortex stretching is the physical mechanism leading to the hypothesized energy cascade from large to small scales. However, Tsinober (2000) noted that in physical space the mechanism of the energy cascade is not exactly due to vortex stretching, but due to vortex compression which contributes to large strain generation. He emphasized the importance of strain (as Kolmogorov
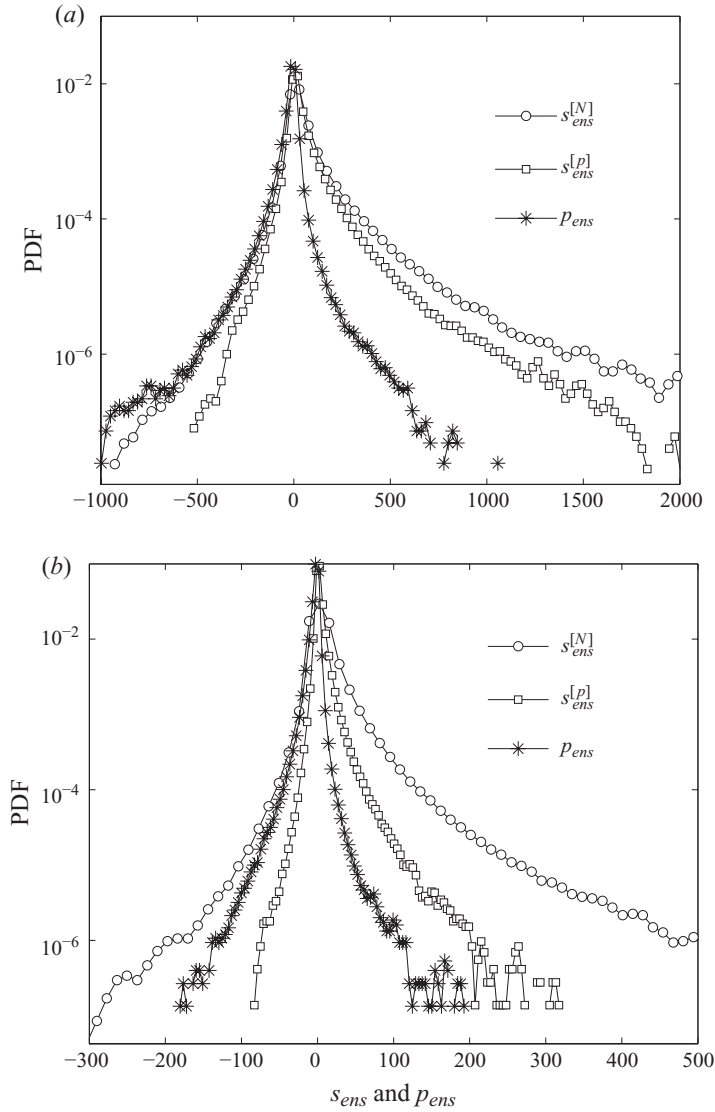
FIGURE 10. Probability distribution of s_{ens} and p_{ens} in DHIT for Newtonian fluid and polymer solution cases ($Wi = 0.62$, $\beta = 0.6$), $s_{ens} = \omega_i S_{ij} \omega_j$, $p_{ens} = \omega_i (\partial^2 T_{mj}^{[p]} / \partial x_m \partial x_n) \epsilon_{nji}$. (a) $t = 0.6$ s; (b) $t = 2$ s.

pointed in 1941) as the vorticity in the context of creation and maintenance of turbulence. So to further investigate the influence on DHIT introduced by polymer additives, we also study the strain field in the Newtonian fluid and polymer solution cases. Firstly, we deduced the mean total strain transport equation for DHIT with polymer additives based on (2.1):

$$\underbrace{\frac{\partial \langle \mathbb{S} \rangle}{\partial t}}_{R_{str}} = \underbrace{-\langle S_{ik} S_{kj} S_{ij} \rangle}_{S_{str}} \underbrace{-\frac{1}{4} \langle \omega_i \omega_j S_{ij} \rangle}_{W_{str}} + \underbrace{\nu^{[s]} \langle S_{ij} \nabla^2 S_{ij} \rangle}_{V_{str}} + \underbrace{\left\langle \frac{\partial^2 T_{ik}^{[p]}}{\partial x_k \partial x_k} S_{ij} \right\rangle}_{P_{str}},$$
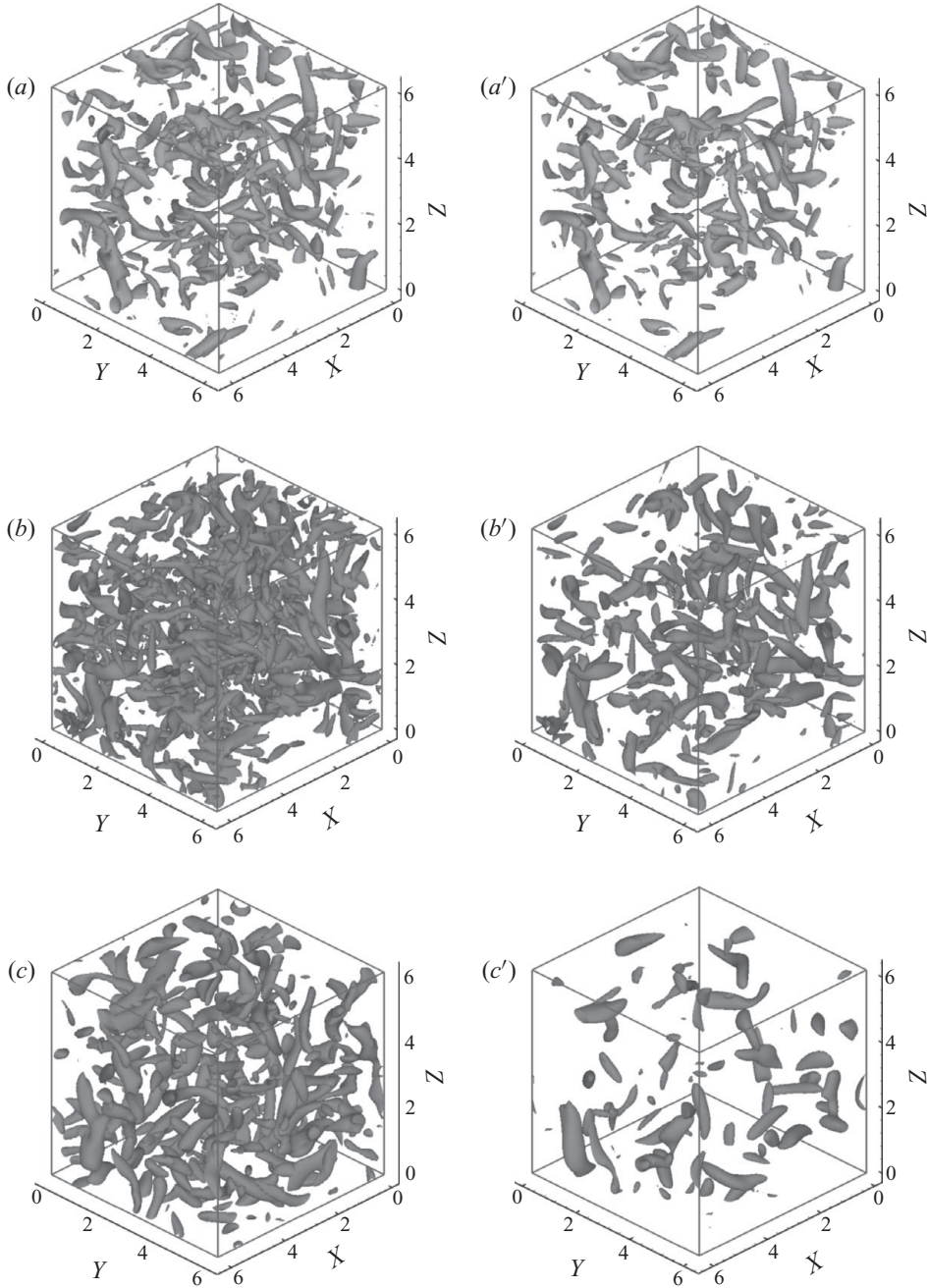
(3.6)

FIGURE 11. Constant Q isosurfaces at different times during EDP in DHIT with and without polymer additives. (a) $t = 0.6$ s, $Q = 20$; (b) $t = 2$ s, $Q = 5$; (c) $t = 5$ s, $Q = 0.8$. (a–c) Newtonian fluid case; (a'–c') polymer solution case, $Wi = 0.62$, $\beta = 0.7$.

where $\mathbb{S} = (1/2)S_{ij}S_{ij}$ is the total strain, R_{str} is the increase rate of $\langle \mathbb{S} \rangle$, S_{str} is the total strain production generated by self-amplification, W_{str} is the enstrophy production effect on the total strain;, V_{str} is the strain viscous dissipation and P_{str} is the polymer effect, which does not appear in the Newtonian fluid case.
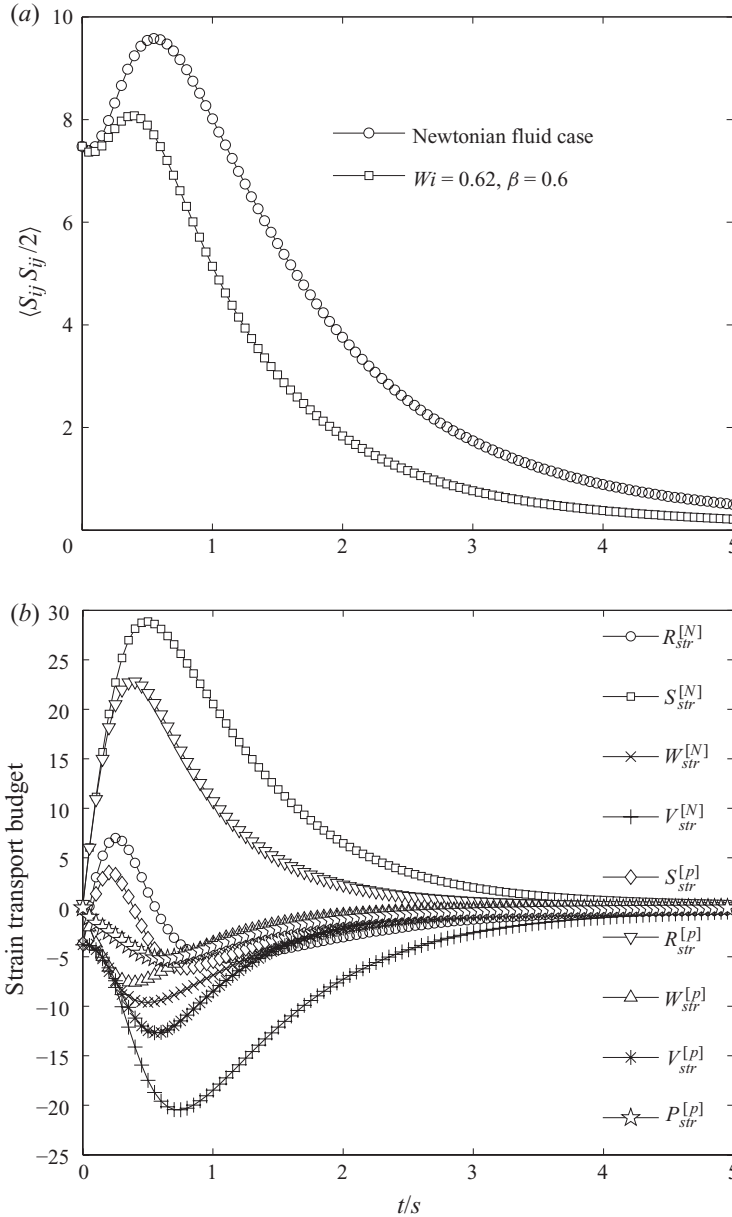
FIGURE 12. Temporal evolution of (*a*) the total strain and (*b*) each term in the strain transport (3.6), $Wi = 0.62$, $\beta = 0.6$.

According to (3.5) and (3.6), we can see that the main source of the enstrophy is from the interaction of vorticity with the strain field, whereas the production of the total strain mainly comes from the self-amplification of the strain field, i.e. $S_{str} = -\langle S_{ik}S_{kj}S_{ij}\rangle$. Moreover, the enstrophy production term, S_{ens}, also appears in (3.6), i.e. $W_{str} = -(1/4)\langle\omega_i\omega_j S_{ij}\rangle = -(1/4)S_{ens}$, showing that vortex stretching tends to suppress the production of the strain, but vortex compression aids it. As is known, energy dissipation is associated precisely with the strain field in both the Newtonian and non-Newtonian fluids. So, we now show the temporal evolution of the total strain and each term in its transport equation in two cases, in figure 12. The results show

that the total strain is smaller in the polymer solution case, indicating that polymers reduce the total strain by elastic stress. With the smaller strain, the turbulent kinetic energy dissipation is decreased (as shown in figure 3*a*). From figure 12(*b*), each term in (3.6) is reduced in the polymer solution case due to the polymer effect. Further, it is noteworthy that the polymer effect term, P_{str}, is marked and negatively skewed (as shown in figure 12*b*), which is the source of the strain reduction. Based on the above analyses of the enstrophy and the strain, we arrive at the following conclusions: in DHIT for polymer solution case, polymer additives suppress not only the stretching of the tube-like vortex structures, but also the strain production due to its elasticity. These two factors are often considered as the impetus of small-scale vortices. As a result, the flow with polymer additives does not display as strong multiscale features as the Newtonian fluid flow, consistent with the results of $E(k)$ (as shown in figure 6*b*).

4. Conclusions

DNS of DHIT with and without polymer additives have been carried out based on Navier–Stokes equations coupled with the FENE-P constitutive model. We studied the influence of polymer additives on DHIT through analysing the Taylor microscale, the decay of total turbulent kinetic energy and energy distribution at each scale in Fourier space, the multiscale intermittency, and the enstrophy and the strain field, respectively. Firstly, an increase of the Taylor microscale is found in DHIT for the polymer solution case, which is the symptom of the drag-reducing effect. Then, the temporal evolution of the balance of energy budget is investigated. It is found that the interaction between turbulence and polymer microstructures leads to larger decay rate of the turbulent kinetic energy in the polymer solution case, i.e. the inhibition of turbulence intensity, or the so-called turbulent DR. An intuitive and natural definition of DR rate for DHIT is proposed based on the integral decay rate of turbulent kinetic energy. Turbulent kineticenergy spectra, $E(k)$, and energy transfer spectra, Im(k), between turbulent structures and polymer microstructures show that $E^{[N]}(k) > E^{[p]}(k)$ at large and intermediate scales and $E^{[p]}(k) \gg E^{[N]}(k)$ at small scales due to the role of Im(k), indicating that the turbulent kinetic energy transfer process for the Newtonian fluid flow becomes unsuitable for the polymer solution case and should be modified especially in the range of scales, where the polymer effect dominates. Analyses of the enstrophy and the strain indicate that both the enstrophy and the strain and their generation terms in polymer solution case are remarkably weaker than in the Newtonian fluid case because of the negative effect of polymer additives, i.e. $P_{ens} < 0$ and $P_{str} < 0$, implying the inhibitive effect on small-scale turbulent vortex structures and the turbulent multiscale property. The visualization of the tube-like vortex structures based on the Q criterion further supports the above results. The investigations of the velocity-derivative skewness and the flatness of velocity fields also support the existence of the drag-reducing effect in DHIT with polymer additives.

REFERENCES

BARNARD, B. J. S. & SELLIN, R. H. J. 1969 Grid turbulence in dilute polymer solutions. *Nature Lond.* **222**, 1160–1162.

BERIS, A. N. & DIMITROPOULOS, C. D. 1999 Pesudospectral simulation of turbulent viscoelastic channel flow. *Comput. Meth. Appl. Mech. Engng* **180**, 365–392.

BERTI, S., BISTAGNINO, A., BOFFETTA, G., CELANI, A. & MUSACCHIO, S. 2006 Small-scale statistics of viscoelastic turbulence. *Europhys. Lett.* **76**, 63–69.

BONN, D., AMAROUCHÈNE, Y., WAGNER, C., DOUADY, S. & CADOT, O. 2005 Turbulent drag reduction by polymers. *J. Phys.: Condens. Matter* **17**, S1195–S1202.

CADOT, O., BONN, D. & DOUADY, S. 1998 Turbulent drag reduction in a closed flow system: boundary layer versus bulk effects. *Phys. Fluids* **10**, 426–436.

CAI, W.-H., LI, F.-C., ZHANG, H.-N., LI, X.-B., YU, B., WEI, J.-J., KAWAGUCHI, Y. & HISHIDA, K. 2009 Study on the characteristics of turbulent drag-reducing channel flow by particle image velocimetry combining with proper orthogonal decomposition analysis. *Phys. Fluids* **21**, 115103.

CANUTO, C., HUSSAINI, M. Y., QUARTERONI, A. & ZANG, T. A. 1988 *Spectral Methods in Fluid Dynamics*. Springer.

CRAWFORD, A., MORDANT, N., XU, H.-T. & BODENSCHATZ, E. 2008 Fluid acceleration in the bulk of turbulent dilute polymer solutions. *New J. Phys.* **10**, 123015.

DE ANGELIS, E., CASCIOLA, C. M., BENZI, R. & PIVA, R. 2002*b* Homogeneous isotropic turbulence in dilute polymers: scale by scale budget. *Chao. Dyn.* (nlin-CD) 0208016.

DE ANGELIS, E., CASCIOLA, C. M., BENZI, R. & PIVA, R. 2005 Homogeneous isotropic turbulence in dilute polymers. *J. Fluid Mech.* **531**, 1–10.

DE ANGELIS, E., CASCIOLA, C. M. & PIVA, R. 2002*a* DNS of wall turbulence: dilute polymers and self-sustaining mechanisms. *Comput. Fluids* **31**, 495–507.

DEN TOONDER, J. M. J., HULSEN, M. A., KUIKEN, G. D. C. & NIEUWSTADT, F. T. M. 1997 Drag reduction by polymer additives in a turbulent pipe flow: numerical and laboratory experiments. *J. Fluid Mech.* **337**, 193–231.

DIMITROPOULOS, C. D., SURESHKUMAR, R. & BERIS, A. N. 1998 Direct numerical simulation of viscoelastic turbulent channel flow exhibiting drag reduction: effect of the variation of rheological parameters. *J. Non-Newtonian Fluid Mech.* **79**, 433–468.

VAN DOORN, E., WHITE, C. M. & SREENIVASAN, K. R. 1999 The decay of grid turbulence in polymer and surfactant solutions. *Phys. Fluids* **8**, 2387–2393.

DOUADY, S., COUDER, Y. & BRACHET, C. M. 1991 Direct observation of the intermittency of intense vorticity filaments in turbulence. *Phys. Rev. Lett.* **67**, 983–986.

DRAPPIER, J., DIVOUX, T., AMAROUCHÈNE, Y., BERTRAND, F., RODTS, S., CADOT, O., MEUNIER, J. & BONN, D. 2006 Turbulent drag reduction by surfactants. *Europhys. Lett.* **74**, 362–368.

DUPRET, F. & MARCHAL, J. M. 1986 Loss of evolution in the flow of viscoelastic fluids. *J. Non-Newtonian Fluid Mech.* **20**, 143–171.

FABULA, A. G. 1966 An experimental study of grid turbulence in dilute high-polymer solutions. PhD thesis, The Pennsylvania State University.

FRIEHE, C. A. & SCHWARZ, W. H. 1970 Grid-generated turbulence in dilute polymer solutions. *J. Fluid Mech.* **44**, 173–193.

DE GENNES, P. G. 1986 Towards a cascade theory of drag reduction. *Physica* A **140**, 9–25.

JEONG, J. & HUSSAIN, F. 1995 On the definition of a vortex. *J. Fluid Mech.* **285**, 69–94.

JIMÉNEZ, J. & WRAY, A. A. 1998 On the characteristics of vortex filaments in isotropic turbulence. *J. Fluid Mech.* **373**, 255–285.

JIN, S. 2007 Numerical simulations of a dilute polymer solution in isotropic turbulence. PhD thesis, Cornell University.

KALELKAR, C., GOVINDARAJAN, R. & PANDIT, R. 2005 Drag reduction by polymer additives in decaying turbulence. *Phys. Rev.* E **72**, 017301.

KOLMOGOROV, A. N. 1991 The local structure of turbulence in incompressible viscous fluid for very large Reynolds number. *Dokl. Akad. Nauk SSSR* 1941, **30**, 9–13 (reprinted in *Proc. R. Soc. Lond.* A **434**, 9–13).

KRAICHNAN, R. H. 1964 Decay of isotropic turbulence in the direct-interaction approximation. *Phys. Fluids* **7**, 1030–1048.

LI, F.-C., KAWAGUCHI, Y. & HISHIDA, K. 2004 Investigation on the characteristics of turbulence transport for momentum and heat in a drag-reducing surfactant solution flow. *Phys. Fluids* **16**, 3281–3295.

LI, F.-C., KAWAGUCHI, Y., HISHIDA, K. & OSHIMA, M. 2006 Investigation of turbulence structures in a drag-reduced turbulent channel flow with surfactant additive using stereoscopic particle image velocimetry. *Exp. Fluids* **40**, 218–230.

LI, F.-C., KAWAGUCHI, Y., SEGAWA, T. & HISHIDA, K. 2005 Reynolds-number dependence of turbulence structures in a drag-reducing surfactant solution channel flow investigated by PIV. *Phys. Fluids* **17**, 075104.

LIBERATORE, M. W., BAIK, S., MCHUGH, A. J. & HANRATTY, T. J. 2004 Turbulent drag reduction of polyacrylamide solutions: effect of degradation on molecular weight distribution. *J. Non-Newtonian Fluid Mech.* **123**, 175–183.

LIBERZON, A., GUALA, M., KINZELBACH, W. & TSINOBER, A. 2006 On turbulent kinetic energy production and dissipation in dilute polymer solutions. *Phys. Fluids* **18**, 125101.

LIBERZON, A., GUALA, M., LÜTHI, B., KINZELBACH, W. & TSINOBER, A. 2005 Turbulence in dilute polymer solutions. *Phys. Fluids* **17**, 031707.

LUMLEY, J. L. 1973 Drag reduction in turbulent flow by polymer additives. *J. Polym. Sci. Macromol. Rev.* **7**, 263–290.

MANSOUR, N. N. & WRAY, A. A. 1994 Decay of isotropic turbulence at low Reynolds number. *Phys. Fluids* **6**, 808–813.

MCCOMB, W. D., ALLAN, J. & GREATED, C. A. 1977 Effect of polymer additives on the small-scale structure of grid-generated turbulence. *Phys. Fluids* **20**, 873–879.

MENG, Q.-G. 2004 On the evolution of decaying isotropic turbulence. *Acta Mechanica Sin.* **20**, 113–116.

MIN, T., YOO, J. Y. & CHOI, H. 2001 Effect of spatial discretization schemes on numerical solution schemes on numerical solutions of viscoelastic fluid flow. *J. Non-Newtonian Fluid Mech.* **100**, 24–47.

OUELLETTE, N. T., XU, H.-T. & BODENSCHATZ, E. 2009 Bulk turbulence in dilute polymer solutions. *J. Fluid Mech.* **629**, 375–385.

PERLEKAR, P., MITRA, D. & PANDIT, R. 2006 Manifestations of drag reduction by polymer additives in decaying, homogenous, isotropic turbulence. *Phys. Rev. Lett.* **97** (264501), 1–4.

PERRY, A. E. & CHONG, M. S. 1987 A description of eddying motions and flow patterns using critical-point concepts. *Annu. Rev. Fluid Mech.* **19**, 125–155.

PTASINSKI, P. K., BOERSMA, B. J., NIEUWSTADT, F. T. M., HULSEN, M. A., VAN DEN BRULE, B. H. A. A. & HUNT, J. C. R. 2003 Turbulent channel flow near maximum drag reduction: simulations, experiments and mechanisms. *J. Fluid Mech.* **490**, 251–291.

PTASINSKI, P. K., NIEUWSTADT, F. T. M., VAN DEN BRULE, B. H. A. A. & HULSEN, M. A. 2001 Experiments in turbulent pipe flow with polymer additives at maximum drag reduction. *Flow Turbul. Combust.* **66**, 159–182.

ROGALLO, R. S. 1981 Numerical experiments in homogeneous isotropic turbulence. *Tech Rep.* 81315. NASA.

SIGGIA, E. D. 1986 Numerical study of small-scale intermittency in three-dimensional turbulence. *J. Fluid Mech.* **107**, 375–406.

SREENIVASAN, K. R. & WHITE, C. M. 2000 The onset of drag reduction by dilute polymer additives and the maximum drag reduction asymptote. *J. Fluid Mech.* **409**, 149–164.

SURESHKUMAR, R. & BERIS, A. N. 1995 Effect of artificial stress diffusivity on the stability of numerical calculations and the flow dynamics of time-dependent viscoelastic flows. *J. Non-Newtonian Fluid Mech.* **60**, 53–80.

SURESHKUMAR, R., BERIS, A. N. & HANDLER, A. H. 1997 Direct numerical simulation of turbulent channel flow of a polymer solution. *Phys. Fluids* **9**, 743–755.

TABOR, M. & DE GENNES, P. G. 1986 A cascade theory of drag reduction. *Europhys. Lett.* **2**, 519–522.

TENNEKES, H. & LUMLEY, J. L. 1972 *A First Course in Turbulence*. MIT Press.

TOMS, B. A. 1949 Some observation on the flow of linear polymer solutions through straight tubes at large Reynolds number. In *Proceedings of First International Congress on Rheology*, vol. 2, pp. 135–141. North-Holland.

Tsinober, A. 2000 Vortex stretching versus production of strain/dissipation. In *Turbulence Structure and Vortex Dynamics* (ed. J. C. R. Hunt & J. C. Vassilicos), pp. 164–191. Cambridge University Press.

Vaithianathan, T. & Collins, L. R. 2003 Numerical approach to simulating turbulent flow of a viscoelastic polymer solution. *J. Comput. Phys.* **187**, 1–23.

Vaithianathan, T., Robert, A., Brasseur, J. G. & Collins, L. R. 2006 An improved algorithm for simulating three-dimensional, viscoelastic turbulence. *J. Non-Newtonian Fluid Mech.* **140**, 3–22.

Walker, D. T. & Tiederman, W. G. 1990 Turbulent structure in a channel flow with polymer injection at the wall. *J. Fluid Mech.* **218**, 377–403.

Warholic, M. D., Heist, D. K., Katcher, M. & Hanratty, T. J. 2001 A study with particle image velocimetry of the influence of drag-reducing polymers on the structure of turbulence. *Exp. Fluids* **31**, 474–483.

Yu, B. & Kawaguchi, Y. 2004 Direct numerical simulation of viscoelastic drag-reducing flow: a faithful finite difference method. *J. Non-Newtonian Fluid Mech.* **116**, 431–466.

Zhong, J., Huang, T. S. & Adrian, R. J. 1998 Extracting 3D vortices in turbulent fluid flow. *IEEE Trans. Pattern Anal. Mach. Intell.* **20**, 193–199.

Zhou, J., Adrian, R. J., Balachandar, S. & Kendall, T. M. 1999 Mechanisms for generating coherent packets of hairpin vortices in channel flow. *J. Fluid Mech.* **387**, 353–396.